PHYSICAL REVIEW B **76**, 045335 (2007)

Valley-orbit splitting in doped nanocrystalline silicon: k·p calculations

Vladimir A. Belyakov and Vladimir A. Burdov
Department of Theoretical Physics, University of Nizhniy Novgorod, Nizhniy Novgorod 603950, Russia

(Received 9 January 2007; revised manuscript received 13 April 2007; published 26 July 2007)

The valley-orbit splitting in silicon quantum dots with shallow donors has been theoretically studied. In particular, the chemical-shift calculation was carried out within the frames of **k**·**p** approximation for single- and many-donor cases. For both cases, the great value of the chemical shift has been obtained compared to its bulk value. Such increase of the chemical shift becomes possible due to the quantum confinement effect in a dot. It is shown for the single-donor case that the level splitting and chemical shift strongly depend on the dot radius and donor position inside the nanocrystal. In the many-donor case, the chemical shift is almost proportional to the number of donors.

DOI: 10.1103/PhysRevB.76.045335 PACS number(s): 73.21.La, 73.20.Hb, 73.22.Dj

I. INTRODUCTION

The ability of silicon nanocrystals to emit electromagnetic energy in the near infrared and even visible range makes them attractive for researchers. Optical properties of the crystallites depend on their shape and size, as well as on the structure defects such as dangling bonds at the nanocrystal surface or impurity centers. The role of the latter has not been studied completely yet.

The goal of the present paper is to find the electron structure of silicon nanocrystals doped with shallow donors. In fact, it is a logical continuation of the two other problems which have been already more or less successfully solved earlier. The first of these two problems is connected with the study of impurity states in bulk semiconductors, in particular, in silicon. Various aspects of this problem have been the subject of detail and successful investigation for several decades. One can find the discussion of the wide range of problems relating to the impurity states in bulk semiconductors, e.g., in Refs. 1–3. The second problem covers electron and optical properties of undoped silicon nanocrystals of small sizes (less than 10 nm). Substantial progress has also been attained in this field for the past 15 years. Carried out theoretical and experimental studies shed light to the structure of electron states and energy spectrum, transition probabilities, mechanism of light emission and absorption in nanocrystals (quantum dots), etc. Integration of these two different problems is interesting in terms of modification of electron and optical properties of silicon quantum dots by their doping with shallow impurities.[4–9]

Investigations of the spatial charge distribution in a quantum dot with impurity,[10] formation of impurity centers inside silicon nanocrystals from the energy point of view,[11] intervalley scattering,[12] hyperfine splitting and optical gap,[13] and screening of the point-charge field[14–20] have been performed in the past years. No doubt, these investigations contributed to more thorough understanding of the properties of the system nanocrystalline Si + impurity. At the same time, a lot of questions are still waiting to be solved. In this paper, we are going to carry out theoretical analysis of electron states in silicon nanocrystals with diameter of 2–5 nm doped with substitutional V-group donors.

Frequently, when considering impurity states in bulk semiconductors, the so-called hydrogenlike model is used. Within this model, the electron potential energy in the donor's field equals

$$V_H = -e^2/\varepsilon_s r, \tag{1}$$

where $-e$ stands for electron charge and ε_s is a dielectric constant of the semiconductor surrounding the donor. However, such a model does not take into account individual features of the embedded donor. In particular, the binding energy is the same for any donor in bulk silicon regardless of the chemical-element number in the Periodic Table. In this case, the number of equivalent valleys in a conduction band determines the degeneracy of the ground-state energy that is sixfold degenerate (without spin). This result is in conflict with the experiment that shows a great difference in binding energies of different donors. Moreover, experiments show the splitting of the sixfold level into a singlet, doublet, and triplet.

Kohn and Luttinger[21,22] explained the divergence of hydrogenlike model and experiments by some extra short-range potential that exists in the nearest vicinity (about the Bohr radius) of the donor nucleus. This supposition was confirmed later by theoretical analysis and calculations.[23,24] Due to the short-range character, this potential is sometimes referred to as the "central-cell correction." Its presence leads to two main consequences. First, because of strong spatial localization, the central-cell potential is weakly localized in **k** space. This provides a mixing of electron states of all the six valleys, which is usually called valley-orbit interaction.[21,22] As a result, the sixfold degenerate energy level splits into three ones corresponding to the singlet, doublet, and triplet with typical splitting energy of about 10–20 meV for various donors. Second, this potential shifts the ground-state energy with respect to the value obtained within the hydrogenlike model, which is known as a chemical shift.

According to Zhou *et al.*[25] and our calculations, in doped quantum dots, the valley-orbit splitting plays a crucial role as well. Similarly to a bulk semiconductor, this leads to the degeneracy removal and chemical shift. Using the local density approximation, the authors of the Ref. 25 have found an anomalously strong splitting (~eV) of the ground-state energy level above the optical gap ("up" states) for silicon quantum dot doped with the V-group donor. That value of the energy splitting highly exceeds the bulk value that is about

©2007 The American Physical Society

10–20 meV as it was already mentioned. Unfortunately, the authors of the Ref. 25 have considered the only structural configuration $\mathrm{Si}_{86}X\mathrm{H}_{76}$ with a single central-located impurity atom X of III or V group. Correspondingly, the nanocrystal size equals 1.6 nm in accordance with the authors' estimations.

In the present paper within the framework of the envelope-function approach, we will obtain the ground-state splitting in the up band of a silicon nanocrystal with a donor. We find the up-state energies as functions of the dot size and donor displacement from the dot center. The wave functions and energies of electrons will be calculated also for many-donor case assuming the homogeneous impurity distribution over the dot volume. We will show that the quantum confinement, increasing as the dot size decreases, is the main reason of the anomalously strong level splitting and chemical shift.

It should be noted that the first-principles calculations of the electronic structure for undoped silicon quantum dots, employing pseudopotential,[26] tight binding,[27,28] or density-functional[29] approaches, exhibit as well a weak splitting (from ~20 to ~5 meV for 2–5 nm nanocrystals) of the ground up-band electron state into a singlet, doublet, and triplet. Such a splitting is also due to the weak valley-orbit interaction and point-group T_d symmetry of the structure.

In contrast to the mentioned above first-principles methods, in the envelope-function approximation, the valley-orbit interaction does not arise automatically. If the $\mathbf{k}\cdot\mathbf{p}$ Hamiltonian does not include a connection between the states of different valleys, the ground-state energy level remains sixfold degenerate.[30,31] We do not attempt to introduce the valley-orbit coupling into the Hamiltonian operator for the quantum dot without donors, since this problem is rather difficult and the splitting is weak. Therefore, we assume that the lowest energy level in undoped quantum dot is sixfold degenerate. In the following, this model will be used as a zeroth order approximation for the quantum dot with a donor (donors).

The paper is organized as follows. First, the single-donor system is considered. For this case, we introduce the electron potential energy in the dot with a donor (Sec. II) and the $\mathbf{k}\cdot\mathbf{p}$ Hamiltonian operator (Sec. III). Basic equations of the problem and a perturbative approach for their solving are formulated in Sec. IV. In Sec. V, we discuss electron states in the case of asymmetric donor position inside the dot. Section VI is devoted to the symmetric donor distribution. Both single- and many-donor cases are considered therein. Eventually, Sec. VII contains some concluding remarks.

II. ELECTROSTATIC POTENTIAL AND SCREENING OF THE ION FIELD

First, we consider the nanocrystal containing one donor. Later, in the Sec. VI, we will generalize the obtained results with the many-donor case.

The starting point of our study is the single-particle Schrödinger equation for an "extra donor's" electron that belongs to the whole nanocrystal after the donor substitutes an atom of silicon in the lattice:

$$H_1|\Psi\rangle = E|\Psi\rangle. \tag{2}$$

Here, the single-particle Hamiltonian operator is

$$H_1 = \frac{\mathbf{p}^2}{2m_0} + V_{latt} + V_C, \tag{3}$$

where m_0 is the free electron mass and V_{latt} is the self-consistent lattice potential. Inside the quantum dot of radius R, the lattice potential is assumed to be coinciding with that for bulk silicon, while outside the dot, it equals infinity. The last term V_C in Eq. (2) represents the Coulomb interaction of the electron with its own image and the donor ion.

Determination of the total Coulomb potential energy V_C in the quantum dot is not a simple task. As it was mentioned in the Introduction, the use of the hydrogenlike model with the macroscopic dielectric constant is obviously insufficient for an analysis of electron states and fine structure of the spectrum. In connection to this, some authors described the screening properties of a nanocrystal with a modified dielectric constant $\varepsilon(R)$ that depends on the dot radius.[16,32] Such a model, indeed, gives some increase of dielectric properties due to the finite size of the crystallite but does not correctly reflect the local structure of the electric field influencing the state of the test electron.

A stricter approach has shown the necessity of self-consistent first-principles calculations of a microscopic charge distribution and electrostatic fields in the nanocrystal.[17,18,20,33] Nevertheless, the obtained microscopic picture permits clear qualitative interpretation using the static dielectric function $\varepsilon(r)$ depending on electron position vector. Calculations of Trani *et al.*[20] have shown that the charge response in the dot remains almost the same as that in the bulk. The authors of Ref. 20 have found the electron density oscillations near the donor ion. However, the oscillations damp the further one gets from the donor in a distance of a few bond lengths. At the same time, some excess positive charge accumulates near the dot boundary. This surface effect that is due to the dangling bonds at the dot boundary explains significant weakening of screening in the nanocrystal.

From the point of view of macroscopic electrodynamics, the above results may be interpreted as follows. The positive point charge polarizes the electron subsystem and causes charge redistribution in the nanocrystal. A negatively charged electron cloud is induced around the donor in a distance of the order of the Bohr radius. Consequently, the same uncompensated positive charge goes to the dot boundary and creates polarization fields which may be treated as the fields of images.

In the case of bulk semiconductor, an explicit form of the electron potential energy in the field of donor's ion has been obtained by Pantelides and Sah.[24] It is convenient to separate it on two components describing the long-range and the short-range parts of the Coulomb interaction. The long-range component represents a macroscopic Coulomb field in a medium. It is described with function (1), where ε_s is silicon permittivity equal to 12. The short-range part $W(\mathbf{r})$ can be expressed as[24]

$$W(\mathbf{r}) = -\frac{e^2}{r}\left(Ae^{-\alpha r} + (1-A)e^{-\beta r} - \frac{e^{-\gamma r}}{\varepsilon_s}\right), \tag{4}$$

where parameters α, β, γ equal 0.7572, 0.3123, and 2.044 of the reciprocal Bohr radius, respectively, and $A=1.175$. The short-range term $W(r)$ represents an interaction of the test electron with the electron cloud having the charge $(1/\varepsilon_s - 1)e$ and the part of the ion charge of the same magnitude and opposite sign. The other part of the ion charge equal to e/ε_s remains unscreened and creates the long-range hydrogenlike field [Eq. (1)] weakened by ε_s times.

Evidently, if the quantum-dot radius considerably exceeds the Bohr radius, the short-range part $W(r)$ does not change its form.[18,20] On the contrary, the long-range part undergoes significant changes in view of the appearance of the polarization fields. As a result, Eq. (1) in a quantum dot transforms into $V(\mathbf{h},\mathbf{r}) = V_{ie}(\mathbf{h},\mathbf{r}) + V_{sp}(r)$, where $V_{ie}(\mathbf{h},\mathbf{r})$ denotes an electron-ion interaction including not only the direct Coulomb attraction but also an interaction between the electron and ion image:

$$V_{ie}(\mathbf{h},\mathbf{r}) = -\frac{e^2}{\varepsilon_s|\mathbf{r}-\mathbf{h}|} - \frac{e^2(\varepsilon_s-\varepsilon_d)}{\varepsilon_s R} \times \sum_{l=0}^{\infty} \frac{h^l r^l}{R^{2l}} \frac{l+1}{l\varepsilon_s + (l+1)\varepsilon_d} P_l(\cos\theta). \tag{5}$$

Here, ε_d is the static dielectric constant of the wide-band matrix surrounding the nanocrystal, $\mathbf{h}$ stands for the donor's position vector, θ is the angle between $\mathbf{r}$ and $\mathbf{h}$, and $P_l(\cos\theta)$ is the Legendre polynomial.

Interaction between the electron and its own image (self-polarization field) depends only on the distance r between the electron and the dot center:

$$V_{sp}(r) = \frac{e^2}{2R}\left(\frac{1}{\varepsilon_d} - \frac{1}{\varepsilon_s}\right) + \frac{e^2(\varepsilon_s-\varepsilon_d)}{2\varepsilon_s(\varepsilon_s+\varepsilon_d)R}\frac{r^2}{R^2-r^2} + \frac{e^2(\varepsilon_s-\varepsilon_d)}{2(\varepsilon_s+\varepsilon_d)^2 R}\ln\left(\frac{R^2}{R^2-r^2}\right) + \frac{e^2(\varepsilon_s-\varepsilon_d)}{2(\varepsilon_s+\varepsilon_d)^2 R}\sum_{n=1}^{\infty}(-\varepsilon)^n s_n(r), \tag{6}$$

where $s_n(r) = \sum_{l=1}^{\infty}(r/R)^{2l}/l^{n+1}$ and $\varepsilon = \varepsilon_d/(\varepsilon_s+\varepsilon_d)$. For typical dielectrics, such as SiO_2 or Al_2O_3, we may set ε_d of the order of 2.5–3. Then, the parameter ε turns out to be 1/5–1/6, which is small enough.

Thus, one can write the Coulomb term V_C in Eq. (3) as the sum $V_C = V(\mathbf{h},\mathbf{r}) + W(\mathbf{h},\mathbf{r})$. Let us formally introduce the local dielectric function $\varepsilon(r)$ in the dot within the framework of macroscopic picture but taking into account the field $W(\mathbf{h},\mathbf{r})$. We consider the central donor location ($h=0$) and write the function $\varepsilon(r)$ as the ratio

$$\varepsilon(r) = -\frac{e^2}{r[V_{ie}(0,\mathbf{r}) + W(0,\mathbf{r})]}. \tag{7}$$

The results of calculations with formula (7) for 1.2 nm nanocrystal are presented in Fig. 1 for $\varepsilon_d=1$. The value $\varepsilon_d=1$ and the nanocrystal size equal to 1.2 nm correspond to the calculations of Trani *et al.*[20] and Ogut *et al.*[17] for a doped silicon nanocrystal $Si_{35}H_{36}$ in vacuum. The results of the Refs. 17 and 20 are also presented in the figure to be compared. One can see a quite good agreement between function (7) and the ones obtained by the local density[20] and pseudopotential[17] methods. This is an evidence in favor of the suggested model for V_C.

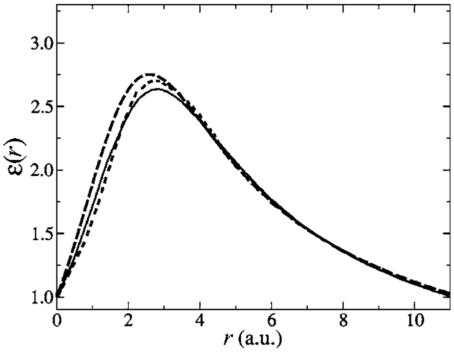

FIG. 1. Dielectric function of the dot vs the distance (in atomic units) from the dot center for $\varepsilon_d=1$. Solid line, present work; dashed line, Trani *et al.* (Ref. 20); dotted line, Ogut *et al.* (Ref. 17).

The case $\varepsilon_d=3$ corresponds to the dielectric surrounding such as SiO_2. This is the case considered in our work. In Fig. 2, we present the dielectric function [Eq. (7)] at $\varepsilon_d=3$ for three different radii of the dot. It is seen that the dielectric function $\varepsilon(r)$ for $\varepsilon_d=3$ is considerably greater than that for $\varepsilon_d=1$. However, the common essential decrease of $\varepsilon(r)$ in a nanocrystal compared to the bulk value takes place. As was pointed out earlier,[15,18,20] such a decrease is mainly due to the polarization charges at the dot boundary, which causes wide decaying area on the dependence $\varepsilon(r)$. The monotonous decrease of $\varepsilon(r)$ goes up to the nanocrystal boundary, where the value of the dielectric function becomes equal to ε_d.

III. HAMILTONIAN OPERATOR OF THE PROBLEM

Direct solving of Eq. (2) is a problem complicated enough. Therefore, it is usually replaced by a more simple approximate method. In the following, we will exploit the

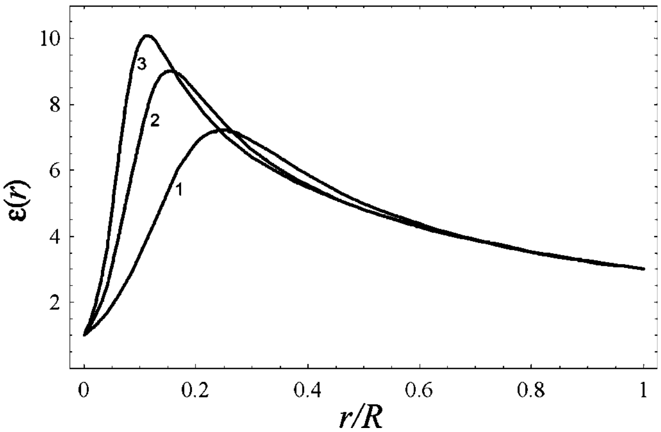

FIG. 2. Dielectric function of the dot at $\varepsilon_d=3$ for (1) $R=1$ nm, (2) $R=1.75$ nm, and (3) $R=2.5$ nm.

$\mathbf{k}\cdot\mathbf{p}$ approach to find the wave function $|\Psi\rangle$ and the electron spectrum.

Let us now construct the $\mathbf{k}\cdot\mathbf{p}$ Hamiltonian operator of the problem. Frequently, when describing various processes in bulk silicon, it is sufficient to consider only one valley in a conduction band but not all the six ones. In this case, the electron wave function is written as a product of a slowly varied envelope function and Bloch function corresponding to the energy minimum of the valley (Δ direction). Accordingly, the $\mathbf{k}\cdot\mathbf{p}$ Hamiltonian is represented as a scalar operator with "longitudinal" $m_l=0.92m_0$ and "transverse" $m_t=0.19m_0$ effective masses in a kinetic-energy term. However, such description is correct if (i) electron energy is close to the band minimum, i.e., obeys the inequality $|E-E_\Delta|\ll|E-E_X|$, where E_X and E_Δ are the energies of the X and Δ points; and (ii) perturbing external fields, such as a donor one, are sufficiently fluent and almost invariable within a unit cell.

The situation we consider is strongly different. Typical size-quantization energies for ~2–5 nm nanocrystals are of the order of the energy difference between X and Δ points or even considerably greater. Besides, the central-cell potential, which we treat as a main reason of the splitting, varies rapidly. In this case, we need the $\mathbf{k}\cdot\mathbf{p}$ Hamiltonian which would correctly describe not only the smallest vicinity of the band minimum but also essentially the wider energy range. Moreover, due to the presence of effective valley-orbit coupling, we should take into account all the six valleys in the conduction band.

At first sight, it seems possible to write the electron wave function in the dot by analogy with the bulk case[24] as the sum over the six valleys:

$$\Psi=\sum_{n=1}^{6}D_n(\mathbf{r})|\Delta_n\rangle. \tag{8}$$

Here, $|\Delta_n\rangle$ are the Bloch functions of the six energy minima, and $D_n(\mathbf{r})$ stand for the slowly varied envelope functions. The Bloch-state basis $|\Delta_n\rangle$ is quite convenient in describing the states with low energies near the dispersion-curve minimum. However, as was already mentioned, the energies we consider are substantially greater. In this case, following Kopylov,[34] we shall use the other Bloch-state basis including six Bloch functions of three different X points in the Brillouin zone. We denote three pairs of these functions as $|X\rangle$, $|X'\rangle$; $|Y\rangle$, $|Y'\rangle$; and $|Z\rangle$, $|Z'\rangle$. Each pair belongs to the twofold degenerate irreducible representation X_1 of the corresponding X point. The Bloch functions without prime have nonzero value at the lattice site, while the primed functions equal zero at those points. The choice of the X_1 functions as the Bloch basis allows us to correctly describe a dispersion-law nonparabolicity that mainly originates from the energy-branch crossing in the X points. As a result, we write the electron wave function in the form

$$\Psi=\sum_{J=X,Y,Z}(F_J|J\rangle+F'_J|J'\rangle), \tag{9}$$

where F_J and F'_J are smooth envelope functions.

In order to obtain the $\mathbf{k}\cdot\mathbf{p}$ Hamiltonian, we have to multiply Eq. (2) by any conjugate Bloch function $\langle J|$ or $\langle J'|$ and then integrate the obtained equation over the unit-cell volume Ω. As a consequence, the external field V_C appears in the $\mathbf{k}\cdot\mathbf{p}$ Hamiltonian in some averaged form.

Since the long-range part $V(\mathbf{h},\mathbf{r})$ is a fluent function, it is strictly diagonal in the Bloch-state basis. The averaging over the unit-cell volume does not change this function, which gives rise in diagonal elements of the $\mathbf{k}\cdot\mathbf{p}$ Hamiltonian.

On the contrary, the central-cell potential varies sharply and contributes in both diagonal and off-diagonal elements. However, averaging over the unit cell yields nonzero only for the unit cell containing the donor. Such elements may be approximated by the Dirac δ functions, as it has been done in Refs. 12 and 35:

$$W_{XY}\equiv\langle X|W|Y\rangle_\Omega=\langle Z|W|X\rangle_\Omega=\langle Y|W|Z\rangle_\Omega=-Q_0\delta(\mathbf{r}-\mathbf{h}),$$

$$W_{AA}\equiv\langle X|W|X\rangle_\Omega=\langle Y|W|Y\rangle_\Omega=\langle Z|W|Z\rangle_\Omega=-Q\delta(\mathbf{r}-\mathbf{h}),$$

$$\begin{aligned}W'_{AA}&\equiv\langle X'|W|X'\rangle_\Omega=\langle Y'|W|Y'\rangle_\Omega=\langle Z'|W|Z'\rangle_\Omega\\&=-Q'\delta(\mathbf{r}-\mathbf{h}).\end{aligned} \tag{10}$$

Here, $\langle A|W|B\rangle_\Omega\equiv\Omega^{-1}\int_\Omega A^*(\mathbf{r})W(\mathbf{h},\mathbf{r})B(\mathbf{r})d\mathbf{r}$, and indices A and B describe the Bloch states X, Y, or Z. Q_0, Q, and Q' are some parameters independent of $\mathbf{r}$ and $\mathbf{h}$, which will be determined below. Since the donor is of substitutional kind, the parameter Q' should be much less than Q_0 and Q because the primed Bloch functions equal zero at the donor site.

The eigenstate and eigenvalue problem is formulated in the form of the Schrödinger-like matrix equation

$$H|\mathbf{F}\rangle\equiv\begin{pmatrix}H_x & U & U\\ U & H_y & U\\ U & U & H_z\end{pmatrix}\begin{pmatrix}F_X\\F'_X\\F_Y\\F'_Y\\F_Z\\F'_Z\end{pmatrix}=E\begin{pmatrix}F_X\\F'_X\\F_Y\\F'_Y\\F_Z\\F'_Z\end{pmatrix}. \tag{11}$$

We have introduced here the matrix Hamiltonian operator H acting in space of the six-dimensional (6D) envelope-function vectors. The origin of the E axis coincides with the X-point energy. Each element of the matrix H is a block 2×2 defined by the following expressions:

$$U=\begin{pmatrix}W_{XY} & 0\\ 0 & 0\end{pmatrix}, \tag{12}$$

$$H_a = \begin{pmatrix} \dfrac{p_a^2}{2m_l} + \dfrac{\mathbf{p}^2 - p_a^2}{2m_t} + V(\mathbf{h},\mathbf{r}) + W_{AA} + U_0(r) & \left(\dfrac{1}{m_t} - \dfrac{1}{m_0}\right) p_b p_c + i\dfrac{p_0}{m_l} p_a \\ \left(\dfrac{1}{m_t} - \dfrac{1}{m_0}\right) p_b p_c - i\dfrac{p_0}{m_l} p_a & \dfrac{p_a^2}{2m_l} + \dfrac{\mathbf{p}^2 - p_a^2}{2m_t} + V(\mathbf{h},\mathbf{r}) + W'_{AA} + U_0(r) \end{pmatrix}. \tag{13}$$

Here, $p_0 \approx 0.14(2\pi\hbar/a_0)$ is the distance in the $\mathbf{p}$ space from any of the energy minima to the nearest X point, and a_0 is the lattice constant of silicon. The confining potential $U_0(r)$ equals zero inside the dot and infinity elsewhere. Each of the small indices (a,b,c) runs over the values x, y, or z and always differs from each other. In the absence of the confining and Coulomb potentials, the matrix [Eq. (13)] transforms into the Kopylov's $\mathbf{k}\cdot\mathbf{p}$ Hamiltonian operator 2×2 written in the Bloch-state basis of a single X point.[34]

In order to completely define the $\mathbf{k}\cdot\mathbf{p}$ Hamiltonian operator H, one needs to find the exact expressions for Q_0, Q, and Q'. All these parameters are, exclusively, the characteristics of the donor core creating the short-range central-cell potential. As it has been mentioned above, its typical scale is the Bohr radius. On this reason, an explicit form of the central-cell potential does not depend, in fact, on the donor surrounding: it is a bulk material or a nanocrystal with the radius significantly exceeding the Bohr radius. Therefore, we may now find the values of Q_0, Q, and Q' from experimental data for the energies of donor levels in bulk silicon.

As has been already mentioned, experiments show the ground-state splitting into singlet with the symmetry of the irreducible representation A_1 of the point group T_d, doublet (E representation), and triplet (T_2 representation). Let us denote the experimentally observed energy shifts related to the sixfold degenerate theoretically calculated value (−31.3 meV according to Faulkner[36]) as $\Delta(A_1)$, $\Delta(E)$, and $\Delta(T_2)$ for the singlet, doublet, and triplet states, respectively, as it is shown in Fig. 3. We define the shift as the difference between the experimental value and the sixfold degenerate theoretical one. The numbers Q_0, Q, and Q' can be found similarly to the method suggested in Refs. 12 and 35. Using the trial function[22] of Kohn and Luttinger, it is easy to express Q_0, Q, and Q' through the above shifts as follows:

$$Q_0 = -\frac{\pi a^2 b}{3}[\Delta(A_1) - \Delta(E)],$$

$$Q = -\frac{\pi a^2 b}{3}[\Delta(A_1) + 2\Delta(E)],$$

$$Q' = -\pi a^2 b \Delta(T_2), \tag{14}$$

where a and b are the variation parameters introduced by Kohn and Luttinger.[22] They are $a = 1.02 a_B$ and $b = 0.58 a_B$, where $a_B = \hbar^2 \varepsilon_s / m_e e^2$ is the effective Bohr radius. In the definition of a_B, the isotropic effective mass m_e has been used. It comes from the averaging of the electron dispersion law in the conduction band over angles: $m_e^{-1} = (2m_t^{-1} + m_l^{-1})/3 \approx (0.26 m_0)^{-1}$.

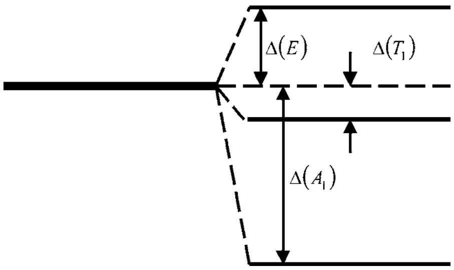

FIG. 3. Schematic representation of the ground-state splitting in bulk silicon.

IV. METHOD OF SOLVING

Solving of the basic equation [Eq. (11)] for no donor case has been described in detail in Ref. 30. The method used there is based on a separation of the Hamiltonian matrix on the main isotropic part H_0 and anisotropic perturbation. The main part called hereafter as the Hamiltonian operator of the zeroth approximation has the form

$$H_0 = \left(\frac{\mathbf{p}^2}{2m_e} + U_0(r)\right) \times \mathbf{I}, \tag{15}$$

where $\mathbf{I}$ is a 6×6 identity matrix. The perturbation equals $H - H_0$ and contains all the terms with zero mean value.

Now, we apply this method to solve our problem, including both the short- and long-range Coulomb terms into the perturbation. The perturbation matrix is written similarly to the total Hamiltonian operator H as follows

$$h = \begin{pmatrix} h_x & U & U \\ U & h_y & U \\ U & U & h_z \end{pmatrix}. \tag{16}$$

The block U is defined as before [Eq. (12)], and the block h_a equals $H_a - H_0^{(2)}$, where $H_0^{(2)}$ coincides with any diagonal block 2×2 of the unperturbed Hamiltonian 6×6 [Eq. (15)].

Because of the isotropic form of the unperturbed Hamiltonian, one may classify its eigenstates similarly to atomic systems as the states of types s, p, d, etc. Then, we expand the envelope-function eigenvector $|\mathbf{F}\rangle$ over this basis with some constant 6D vector coefficients to be determined

$$|\mathbf{F}\rangle = |\mathbf{C}_s\rangle|s\rangle + \sum_{a=x,y,z} |\mathbf{C}_p^{(a)}\rangle|p_a\rangle + \sum_{i=1}^{5} |\mathbf{C}_d^{(i)}\rangle|d_i\rangle + \cdots . \tag{17}$$

Here, $|s\rangle$, $|p_a\rangle$, $|d_i\rangle$, etc., are the s-, p-, d-type, etc., eigenstates of the unperturbed operator [Eq. (15)].

As was shown in Ref. 30, it is sufficient to keep in the expansion [Eq. (17)] only the s and p states to determine the ground-state envelope functions, because all the other unperturbed states have too high energies and weakly mix with the lowest states. After this simplification, the matrix differential equation [Eq. (11)] transforms into the algebraic ones:

$$(E - E_0 - \langle s|h|s\rangle)|\mathbf{C}_s\rangle = \sum_{a=x,y,z} \langle s|h|p_a\rangle|\mathbf{C}_p^{(a)}\rangle,$$

$$(E - E_1 - \langle p_a|h|p_a\rangle)|\mathbf{C}_p^{(a)}\rangle = \langle p_a|h|s\rangle|\mathbf{C}_s\rangle + \sum_{b\neq a} \langle p_a|h|p_b\rangle|\mathbf{C}_p^{(b)}\rangle. \tag{18}$$

Here, $E_0 = \hbar^2\pi^2/2m_eR^2$ and $E_1 = \hbar^2\mu^2/2m_eR^2$ are the eigenvalues of the unperturbed s and p states, respectively, and $\mu \approx 4.4934$ is the first root of the spherical Bessel function $j_1(x)$.

In order to proceed with Eq. (18), we have to calculate the matrix elements of s-s, s-p, or p-p type for all terms of the perturbation matrix h. Below, we write down the nonzero matrix elements which are necessary for the subsequent calculations. In particular, the matrix elements of the central-cell operators [Eq. (10)] are given by

$$\langle s|W|s\rangle = -\tilde{Q}\frac{\pi j_0^2(\pi q)}{2R^3},$$

$$\langle s|W|p_a\rangle = -\tilde{Q}\frac{\sqrt{3}n_a}{2R^3 j_0(\mu)} j_0(\pi q) j_1(\mu q),$$

$$\langle p_b|W|p_a\rangle = -\tilde{Q}\frac{3n_a n_b j_1^2(\mu q)}{2\pi R^3 j_0^2(\mu)}, \tag{19}$$

where $q = h/R$, $n_a = h_a/h$. W is any of the operators in Eq. (10), and $\tilde{Q}$ is the corresponding parameter. Anisotropic terms of the bulk Hamiltonian matrix also give rise to the perturbation. Their matrix elements are as follows:

$$i\frac{p_0}{m_l}\langle p_x|p_x|s\rangle = i\frac{p_0}{m_l}\langle p_y|p_y|s\rangle = i\frac{p_0}{m_l}\langle p_z|p_z|s\rangle = \frac{2\hbar p_0}{\sqrt{3}m_l R}\frac{\pi\mu}{\mu^2 - \pi^2} \equiv H_{sp},$$

$$\langle p_x|\mathbf{p}^2 - 3p_z^2|p_x\rangle = \langle p_y|\mathbf{p}^2 - 3p_z^2|p_y\rangle = -\frac{\langle p_z|\mathbf{p}^2 - 3p_z^2|p_z\rangle}{2} = \frac{\hbar^2}{R^2}\frac{2\mu^2}{5} \equiv \frac{6m_t m_l}{m_l - m_t}H_{pp}. \tag{20}$$

Finally, the long-range part of the Coulomb interaction has matrix elements of the following kind:

$$\langle s|V(\mathbf{h},\mathbf{r})|s\rangle = \frac{e^2}{2R}\left(\frac{1}{\varepsilon_d} - \frac{1}{\varepsilon_s}\right) + 0.2\frac{e^2}{\varepsilon_s R} - \frac{e^2}{R}\left[\frac{1}{\varepsilon_d} - \frac{1}{\varepsilon_s}\left(\frac{\sin(2\pi q)}{2\pi q} - J(2\pi, 2\pi q)\right)\right] \equiv V_{ss}(q),$$

$$\langle p_a|V(\mathbf{h},\mathbf{r})|p_a\rangle = \frac{e^2}{2R}\left(\frac{1}{\varepsilon_d} - \frac{1}{\varepsilon_s}\right) + 0.29\frac{e^2}{\varepsilon_s R} - \frac{e^2}{R}\left[\frac{1}{\varepsilon_d} - \frac{1}{\varepsilon_s \sin^2\mu}\left(2\cos^2\mu - \frac{\sin(2\mu q)}{2\mu q} - \frac{\sin^2(\mu q)}{(\mu q)^2} + J(2\mu, 2\mu q)\right)\right] \equiv V_{pp}(q),$$

$$\begin{aligned}\langle s|V(\mathbf{h},\mathbf{r})|p_a\rangle = \frac{8\pi}{\sqrt{3}}\frac{e^2 n_a}{\varepsilon_s R}\Bigg\{&\frac{\cos(\pi q)\cos(\mu q)}{2q(\mu^2 - \pi^2)\sin\mu} + \frac{\mu^2 + \pi^2}{\mu^2 - \pi^2}\frac{\sin(\pi q)\sin(\mu q)}{4\pi\mu q\sin\mu} - \frac{q}{4\mu} - \left(\frac{1}{2} + \frac{3\mu^2 - \pi^2}{q^2(\mu^2 - \pi^2)^2}\right)\frac{\cos(\pi q)\sin(\mu q)}{2\mu\sin\mu}\\ &+ \left(1 + \frac{4\mu^2}{q^2(\mu^2 - \pi^2)^2}\right)\frac{\cos(\mu q)\sin(\pi q)}{4\pi\sin\mu} - q\frac{\mu^2 - \pi^2}{8\pi\mu\sin\mu}[J(\mu + \pi, \mu - \pi) - J((\mu + \pi)q, (\mu - \pi)q)]\\ &+ \frac{\varepsilon_s - \varepsilon_d}{\varepsilon_s + 2\varepsilon_d}\frac{\mu q}{(\mu^2 - \pi^2)^2}\Bigg\} \equiv V_a(q).\end{aligned} \tag{21}$$

The numbers 0.2 and 0.29 in Eq. (21) come from the numerical integration, $J(y,x) = \int_x^y dt[1 - \cos(t)]/t$. We should note that the term $\langle p_a|V(\mathbf{h},\mathbf{r})|p_a\rangle$ has some nonzero anisotropic addition, which has not been included into expressions (21). Also, matrix elements $\langle p_a|V(\mathbf{h},\mathbf{r})|p_b\rangle$, with $a \neq b$, have not been presented here. However, both these terms are negligibly small. We omit them in order to simplify the cumbersome expressions for the matrix elements.

V. ASYMMETRIC DONOR POSITION

Generally speaking, Eq. (18) is solved numerically except for the two special cases of spherical symmetry. If the donor occupies some arbitrary position inside the dot, any symmetry in the structure is absent. The main result in this case is the total degeneracy removal. Consequently, the ground state in the dot splits into six different states. The solutions of Eqs. (18) for this case have been obtained by the computational methods. As a result, the energies of the six "lowest" states

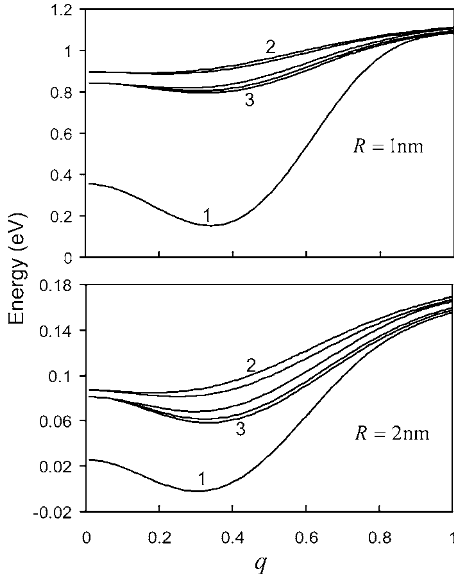

FIG. 4. Energies of the (1) singlet, (2) doublet group, and (3) triplet group states with respect to the X-point energy in a conduction band of silicon as functions of the phosphorus-donor displacement from the dot center. $n_x=0.8$, $n_y=0.5$, and $n_z=0.3$.

are shown in Fig. 4 as functions of the dimensionless donor displacement q from the dot center for two different dot radii.

One can see that the twofold and threefold levels weakly split into two or three levels, respectively, if $q\neq 0$. As q increases, their energies slowly rise. The energy of the ground state drops to some minimal value and then rises approaching the doublet and triplet groups of levels. At the point of the ground-state energy minimum, the level splitting in the nanocrystal becomes maximal, since the off-diagonal matrix elements of s-p-type $V_a(q)$ have maximal values. Such a splitting is a consequence of the strong entanglement of all the six states, which is accompanied by the "repulsion" of their energy levels.

We have calculated the electron wave functions of the six lowest states for $q_x=0.24$, $q_y=0.15$, $q_z=0.1$. Chosen values of q_a correspond to some arbitrary donor position that has no any symmetry with respect to the basic crystallographic directions and the dot boundary. As the calculations show, the ground electron state has the wave function being predominantly a product of the s-type envelope function and Bloch function $|A_1\rangle=(|X\rangle+|Y\rangle+|Z\rangle)/\sqrt{3}$. The latter belongs to the irreducible representation A_1 of the point group T_d. For $R=2$ nm, the quota of this term in the ground electron state equals 0.7, while the quotas of the products $|p_x\rangle|A_1\rangle$, $|p_y\rangle|A_1\rangle$, and $|p_z\rangle|A_1\rangle$ equal 0.11, 0.04, and 0.014, respectively. Thus, the overall "weight" of the Bloch state $|A_1\rangle$ in the ground-state wave function is approximately 0.9. The remaining 10% is almost homogeneously distributed over the Bloch states $|X'\rangle$, $|Y'\rangle$, and $|Z'\rangle$, which are the functions of the irreducible representation T_2 of the T_d group. At the same time, the Bloch states $|E^{(1)}\rangle=(|X\rangle-|Y\rangle)/\sqrt{2}$ and $|E^{(2)}\rangle=(|X\rangle+|Y\rangle-2|Z\rangle)/\sqrt{6}$, transformed in accordance with the irreducible representation E of the tetrahedral group, are not involved into the ground state. The similar situation takes place for the ground state in the symmetric case $q=0$ [see expression for Ψ_1 in Eq. (24) below], in which the Bloch functions $|E^{(1,2)}\rangle$ are absent. On the other hand, in the symmetric case, the products $|p_a\rangle|A_1\rangle$ do not appear in the ground state. That is in contrast with the asymmetric case.

Figure 5 shows the quota of the s-type envelope function in the ground state versus the dot radius in the asymmetric and symmetric cases for $q=0.3$ and $q=0$, respectively. The dashed line indicates the weight of the s-type envelope function for $q=0.3$. As is seen, the breakdown of the spherical symmetry in the system reduces the quota of the s-type part compared to that for $q=0$ (upper curves in Fig. 5). Correspondingly, the p-state weight rises.

VI. SYMMETRIC DONOR POSITION

Now, we present some general analytical expressions for the symmetric case. For example, it is easy to find an analytical solution of Eq. (18) if a single donor occupies the dot center, or the great amount of donors is almost uniformly distributed over the dot volume.

In these symmetric cases, system (18) is simplified because all the off-diagonal s-p-type matrix elements vanish. Solving of system (18) exhibits the splitting of the ground electron state in the dot into the singlet, doublet, and triplet, as it was in the bulk. Related to the X-points, the energies of these states are written in the form

$$E^{(j)} = \bar{E} + \bar{V} - H_{pp} + \frac{W_j^{(+)}}{2} - \sqrt{\left(\frac{\delta E + \delta V - W_j^{(-)}}{2} - H_{pp}\right)^2 + H_{sp}^2}. \qquad (22)$$

Here, index j enumerates the levels of the singlet ($j=1$), doublet ($j=2$), and triplet ($j=3$) whose energies differ from each other due to the presence of the central-cell potential. We have introduced in Eq. (22) the mean values of the size-quantization energy and long-range Coulomb matrix element: $\bar{E}=(E_0+E_1)/2$ and $\bar{V}=(\langle s|V(\mathbf{h},\mathbf{r})|s\rangle+\langle p|V(\mathbf{h},\mathbf{r})|p\rangle)/2$, respectively. The notation $\langle p|\cdots|p\rangle$ means, in fact, $\langle p_a|\cdots|p_a\rangle$ with any of the p-type envelope functions. δE is the difference of E_1 and E_0, and $\delta V=\langle p|V(\mathbf{h},\mathbf{r})|p\rangle-\langle s|V(\mathbf{h},\mathbf{r})|s\rangle$. At last, the matrix elements of the central-cell potential for the singlet, doublet, and triplet states are defined by

$$W_1^{(\pm)} = \langle s|(2W_{XY} + W_{AA})|s\rangle \pm \langle p|W'_{AA}|p\rangle,$$

$$W_2^{(\pm)} = \langle s|(W_{AA} - W_{XY})|s\rangle \pm \langle p|W'_{AA}|p\rangle,$$

$$W_3^{(\pm)} = \langle s|W'_{AA}|s\rangle \pm \langle p|W_{AA}|p\rangle. \qquad (23)$$

Explicit expressions for $\bar{V}$, δV, and $W_j^{(\pm)}$ are, of course, different for the single- and many-donor cases. We will present them below when discussing each of these cases.

The electron wave functions of the singlet, doublet, and triplet are described by the following expressions:

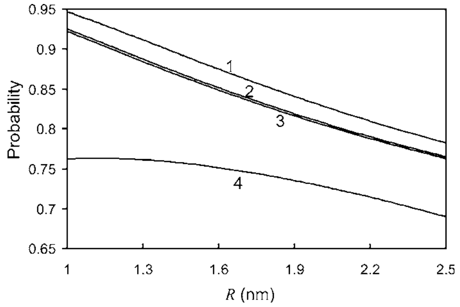

FIG. 5. The weight of the s-type envelope function in the electron state. Upper curves—$q=0$: 1, singlet state; 2, doublet states; 3, triplet states. 4, The weight of the s-type envelope function in the ground electron state for asymmetric donor position: $q_x=0.24$, $q_y=0.15$, and $q_z=0.1$.

$$\Psi_1=\cos(\lambda_1)|A_1\rangle|s\rangle+\sin(\lambda_1)\frac{|X'\rangle|x\rangle+|Y'\rangle|y\rangle+|Z'\rangle|z\rangle}{\sqrt{3}},$$

$$\Psi_2^{(1)}=\cos(\lambda_2)|E^{(1)}\rangle|s\rangle+\sin(\lambda_2)\frac{|X'\rangle|x\rangle-|Y'\rangle|y\rangle}{\sqrt{2}},$$

$$\Psi_2^{(2)}=\cos(\lambda_2)|E^{(2)}\rangle|s\rangle+\sin(\lambda_2)\frac{|X'\rangle|x\rangle+|Y'\rangle|y\rangle-2|Z'\rangle|z\rangle}{\sqrt{6}},$$

$$\Psi_3^{(1)}=\cos(\lambda_3)|X'\rangle|s\rangle-\sin(\lambda_3)\frac{\sqrt{2}|A_1\rangle+\sqrt{3}|E^{(1)}\rangle+|E^{(2)}\rangle}{\sqrt{6}}|x\rangle,$$

$$\Psi_3^{(2)}=\cos(\lambda_3)|Y'\rangle|s\rangle-\sin(\lambda_3)\frac{\sqrt{2}|A_1\rangle-\sqrt{3}|E^{(1)}\rangle+|E^{(2)}\rangle}{\sqrt{6}}|y\rangle,$$

$$\Psi_3^{(3)}=\cos(\lambda_3)|Z'\rangle|s\rangle-\sin(\lambda_3)\frac{|A_1\rangle-\sqrt{2}|E^{(2)}\rangle}{\sqrt{3}}|z\rangle. \quad (24)$$

The parameter λ_j defines the weight of the s- or p-type envelope function in the electron state. Its value is given by

$$\cos(2\lambda_j)=\frac{\delta E+\delta V-2H_{pp}-W_j^{(-)}}{\sqrt{(\delta E+\delta V-2H_{pp}-W_j^{(-)})^2+4H_{sp}^2}}. \quad (25)$$

Actually, all the parameters λ_j vary within the range $0\leqslant\lambda_j\leqslant\pi/2$.

In the bulk Si, the wave functions of the six lowest donor states are the products of the $|A_1\rangle$, $|E\rangle$, or $|T_2\rangle$ Bloch functions and s-type envelope function.[24,36] In the quantum dot, the situation is different. The strong quantum confinement involves into the electron states extra terms with p-type envelope functions, which reduce the weight of the s-type terms. Consequently, the spherical symmetry of the envelope functions disappears. This is an important distinguishing feature of splitting in nanocrystal compared to the one in bulk. In the case $\lambda_j=0$, the spherical symmetry of the envelope functions is completely restored because the p-type terms vanish.

Thus, the electron wave function becomes a sum of two parts. The first part has the bulklike form, while the second part with the p-type envelope functions has a more complicated structure. Nevertheless, the total wave function belongs to the corresponding irreducible representation of the tetrahedral group as it was in the bulk. One can determine the quota of the first part in the singlet, doublet, and triplet electron states as the probability to be in the s state: $P^{(j)}=\cos^2(\lambda_j)$. These probabilities will also be discussed below for both symmetric cases.

A. Single-donor case

The general expressions for the energies and wave functions of the singlet, doublet, and triplet electron states in the quantum dot have already been obtained [see Eqs. (22)–(25)]. Now, we should define all the matrix elements introduced in Eqs. (22)–(25) for the case of the central-located single donor in the dot.

The s-p and p-p matrix elements of the central-cell potential equal zero, while the s-s matrix elements are group in accordance with the symmetry of the T_d-group representations. Taking into account Eqs. (10) and (14), this yields

$$W_1^{(\pm)}=\langle s|(2W_{XY}+W_{AA})|s\rangle=\frac{\pi^2a^2b}{2R^3}\Delta(A_1),$$

$$W_2^{(\pm)}=\langle s|(W_{AA}-W_{XY})|s\rangle=\frac{\pi^2a^2b}{2R^3}\Delta(E),$$

$$W_3^{(\pm)}=\langle s|W'_{AA}|s\rangle=\frac{\pi^2a^2b}{2R^3}\Delta(T_2). \quad (26)$$

Since $q=0$ for the central donor position, the s-p matrix elements of the long-range field $V_a(q)$ equal zero, while the s-s and p-p matrix elements have nonzero values. Correspondingly, $\bar{V}$ and δV are defined as $\bar{V}=[V_{ss}(0)+V_{pp}(0)]/2$ and $\delta V=V_{pp}(0)-V_{ss}(0)$.

It is known that in bulk Si, the energy shift of the ground state is usually considerably greater than those for the doublet and triplet states. Therefore, it is natural to expect the stronger shift of the singlet level compared to the other ones in quantum dots as well. This is confirmed by the solutions [Eq. (22)] shown in Fig. 6.

It is seen that the energy of the singlet state (line 1 in the figure) for three chemical elements being typical donors for silicon is always strongly split off. On the contrary, the doublet and triplet states (lines 2 and 3, respectively) have the energies close to each other, as well as to the sixfold degenerate energy of the ground state in the case of no valley-orbit interaction (dashed line in Fig. 6). The difference between line 1 and the dashed line coincides with the chemical shift. As it follows from the figure, an introduction of arsenic in the nanocrystal provides maximal chemical shift, while the shift produced by antimony is almost two times less. Some intermediate shift values have been obtained for the dot doped with phosphorus.

Despite the fact that the matrix elements [Eq. (26)] of the valley-orbit interaction for nanocrystal turn out to be directly proportional to the "bulk" values of the energy shifts, the splitting in nanocrystal is not proportional to that in bulk.

This is due to the complicated nonlinear dependence of $E^{(j)}$ on $W_j^{(\pm)}$. In turn, such nonlinear dependence arises from a mixing of the s- and p-type unperturbed envelope functions in the quantum states of a doped dot.

It is also seen in Fig. 6 that the chemical shift becomes greater for smaller nanocrystals. This circumstance was pointed out earlier for doped dots in connection with the calculations of hyperfine splitting[13] and electronic structure[25] of the nanocrystal $\mathrm{Si}_{86}X\mathrm{H}_{76}$. Such behavior is explained by the enhanced quantum confinement effect. The envelope function of the lowest energy level is mainly of the s type. At the same time, the Bloch function is predominantly of the A_1 type, i.e., it has nonzero value at the donor site. It is well known that the envelope function in a spherical potential well has the normalization factor $\sim R^{-3/2}$. As a result, the total wave function at the center of the dot significantly increases if the dot size decreases. Correspondingly, the matrix elements of the central-cell potential defining the shift of the ground-state energy rise quickly. Meanwhile, independent of the envelope-function type, the Bloch functions for the excited states have mainly E or T_2 symmetry. These functions equal zero at the donor site. Consequently, the matrix elements $\langle A|W|B\rangle_\Omega$, where $|A\rangle$ and $|B\rangle$ stand for E or T_2 type functions, are considerably smaller compared to the one for the ground state. This leads to the smaller values of the energy shifts for the doublet and triplet states and enhancement of the level splitting shown in the figure.

It was already mentioned that the density-functional theory[25] also gives the strong splitting of the lowest level in the $\mathrm{Si}_{86}X\mathrm{H}_{76}$ nanocrystal with the central-located donor atom X. We have attempted to compare our results on the energy splitting with the values reported by the authors of Ref. 25. However, their calculations have been performed for the nanocrystal with too small size of about 1.6 nm. The applicability of the $\mathbf{k}\cdot\mathbf{p}$ method for such small nanocrystals is, of course, questionable. Nevertheless, we have calculated the energy splitting for 1.6 nm nanocrystal by the method used in the present paper.

Surprisingly, we have found a quite good agreement between the two works. For instance, the differences between the doublet (upper) and triplet (middle) energy levels in the Ref. 25 are about 0.07, 0.11, and 0.15 eV for phosphorus, arsenic, and antimony donor, respectively. The same energies calculated by the $\mathbf{k}\cdot\mathbf{p}$ method used here for 1.6 nm quantum dot turn out to be 0.11, 0.11, and 0.2 eV for these three dopants. The singlet-doublet transition energy in the density-functional theory[25] has the values 1.12 eV (P), 1.22 eV (As), and 1.07 eV (Sb), while the $\mathbf{k}\cdot\mathbf{p}$ method yields 1.12 eV (P), 1.87 eV (As), and 1.11 eV (Sb). Evidently, only the singlet-doublet transition energy for arsenic has an overestimate value in the frames of the $\mathbf{k}\cdot\mathbf{p}$ method. At the same time, all the other splitting energies exhibit quite satisfactory (within a few percent) coincidence.

The probabilities $P^{(j)}$ as functions of the dot radius are plotted in Fig. 5 (upper lines 1–3 in the figure). It is seen that the ground singlet state has the greatest weight of the s-type part compared to the other states. This weight is large but gradually drops with increasing the dot radius, as well as for the doublet and triplet states. Evidently, from the symmetry point of view, the bulk and the "dot" systems are not so far from each other. This is, of course, a consequence of the symmetric donor position in the dot.

B. Many-donor case

Let us now consider the opposite situation to the one explored in the previous section. Accordingly, we suppose a great number of donors in the dot: $N \gg 1$. In order to examine this case, several important assumptions will be made.

First, the nanocrystal is treated as a neutral dot, i.e., we assume that all the electrons emitted from the donors are kept inside the nanocrystal. Second, the spatial donor distribution is assumed to be homogeneous over the quantum-dot volume, and no donors are outside the dot. Finally, we apply the Hartree-like approximation to describe the "slow" Coulomb field $V(\mathbf{r})$. Thus, each of the N electrons within the nanocrystal is subjected to the self-consistent electric field of the N ions, other $N-1$ electrons, and the central-cell fields of all the donors.

The Hartree procedure is equivalent to solving the single-particle Schrödinger equation like Eq. (2), in which the smooth part of the potential energy $V(\mathbf{r})$ obeys the Poisson equation

$$\mathrm{div}(\varepsilon(\mathbf{r})\,\nabla\, V(\mathbf{r})) = 4\pi e\rho(\mathbf{r}), \tag{27}$$

where e the is positive elementary charge and $\rho(\mathbf{r})$ is the charge density. Following the rigorous Hartree method, one would write the function $\rho(\mathbf{r})$ as the sum of two parts: $\rho(\mathbf{r}) = \rho_i(\mathbf{r}) + \rho_e(\mathbf{r})$, where $\rho_i(\mathbf{r})$ and $\rho_e(\mathbf{r})$ are charge densities of the N donor ions and $N-1$ electrons. Generally speaking, the Hartree method represents some converged procedure based on subsequent iterations in electron wave function and potential energy. As a rule, such procedure requires a computational technique and becomes more and more complicated upon increasing the number of particles considered.

Instead, a certain simplified model will be used to solve the Poisson equation [Eq. (27)]. We assume the total charge density $\rho(\mathbf{r})$ to be independent of $\mathbf{r}$ within the quantum dot and equal to zero outside the dot. It means that uncompensated charge $+e$ arising from the N donor ions and $N-1$ electrons is distributed homogeneously over the dot volume. In this case, the density of charge is written as

$$\rho(\mathbf{r}) = \rho(r) = \frac{3e}{4\pi R^3}\Theta(R-r), \tag{28}$$

where $\Theta(R-r)$ is the step function. Of course, it is not so in reality, but finding of corrections to Eq. (28) is a sufficiently laborious work not leading, however, to significant changes in the electron energies and wave functions.

The solution of the Poisson equation [Eq. (27)] with the charge density [Eq. (28)] has the form

$$V(r<R) = \frac{e^2r^2}{2\varepsilon_s R^3} - \frac{e^2}{2\varepsilon_s R} - \frac{e^2}{2\varepsilon_d R},$$

$$V(r>R) = -\frac{e^2}{\varepsilon_d r}. \tag{29}$$

Since the barriers at the dot boundary are assumed to be infinitely high, we are interested only in the function $V(r$

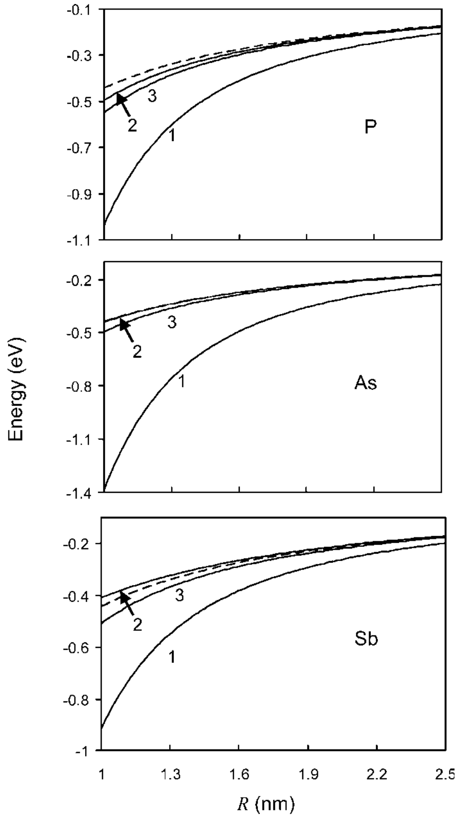

FIG. 6. Energies of the (1) singlet, (2) doublet, and (3) triplet electron states in a quantum dot with a donor related to the sixfold degenerate ground-state energy in the dot without donor. The donor occupies the dot center. The dashed line represents the shift of the ground-state level in the case of no valley-orbit interaction in the system. For the dot doped with arsenic, the dashed line almost coincides with the doublet-state energy.

$<R$). It rises from the dot center as a parabolic function, and its total change on the scale R equals $e^2/2\varepsilon_s R$, which is of the order of a few tens of meV.

Because of the isotropic form of the function $V(\mathbf{r})$, the off-diagonal matrix elements $\langle s|V(\mathbf{r})|p_a\rangle$ and $\langle p_b|V(\mathbf{r})|p_a\rangle$ for $a \neq b$ equal zero, while the diagonal matrix elements $\langle s|V(\mathbf{r})|s\rangle$ and $\langle p_a|V(\mathbf{r})|p_a\rangle$ have close nonzero values equal to

$$\langle s|V(\mathbf{r})|s\rangle = -\frac{e^2}{\varepsilon_d R} - \frac{e^2}{3\varepsilon_s R}\left(1 + \frac{3}{4\pi^2}\right),$$

$$\langle p_a|V(\mathbf{r})|p_a\rangle = -\frac{e^2}{\varepsilon_d R} - \frac{e^2}{3\varepsilon_s R}\left(1 - \frac{2}{\mu^2}\right). \qquad (30)$$

Thus, the screened Coulomb field in the many-donor case leads, mainly, to the common shift of all the levels, which equals approximately $\bar{V}=-e^2[1/\varepsilon_d+(1+3/8\pi^2-1/\mu^2)/3\varepsilon_s]/R$. Meanwhile, the relative shift of the s- and p-levels, defined by the difference between p-p and s-s matrix elements [Eq. (30)] and giving rise to the level splitting, does not exceed several meV. This value is much less than any other typical energy of the problem such as, e.g., the splitting energy due to the valley-orbit coupling, which is about several tenths of eV or even more according to the previous results. Therefore, it is obvious that any other (more accurate) form of the charge $(+e)$ distribution inside the nanocrystal will give the same-order contribution into the potential energy and level splitting, which should be estimated presumably as very weak. In what follows, we neglect this contribution in the splitting and assume the matrix elements [Eq. (30)] to be the same and equal to $\bar{V}$.

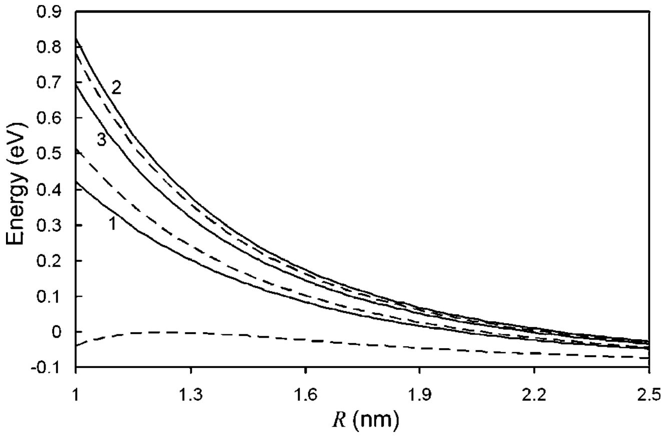

FIG. 7. Energy splitting in the quantum dot with $N=5$ (solid curves) and $N=10$ (dashed curves) donors. 1, singlet state; 2, doublet states; 3, triplet states.

In contrast to this, the valley-orbit coupling gives indeed a substantial rise in the ground-state splitting and chemical shift as it took place for the single-donor case. It is clear that the Poisson equation describes only the long-range field and does not take into account the central-cell corrections. Therefore, it is necessary to calculate them separately. We can easily obtain the matrix elements of the central-cell potential as a spatial mean value of expressions (19) multiplied by N. This yields

$$\langle s|W|s\rangle = \langle p_a|W|p_a\rangle = -\tilde{Q}n,$$

$$\langle s|W|p_a\rangle = \langle p_a|W|p_b\rangle = 0, \qquad (31)$$

where $n=3N/4\pi R^3$ is the donor concentration. W implies here any linear combination of the operators in Eq. (10), and $\tilde{Q}$ is the corresponding combination of the numbers Q_0, Q, and Q'. In particular, the parameters $W_j^{(\pm)}$ from Eq. (20) are as follows:

$$W_1^{(\pm)} = -n(2Q_0 + Q \pm Q') = \pi a^2 b[\Delta(A_1) \pm \Delta(T_2)],$$

$$W_2^{(\pm)} = -n(Q - Q_0 \pm Q') = \pi a^2 b[\Delta(E) \pm \Delta(T_2)],$$

$$W_3^{(\pm)} = -n(Q' \pm Q) = \frac{\pi a^2 b}{3}[3\Delta(T_2) \pm \Delta(A_1) \pm 2\Delta(E)]. \qquad (32)$$

Notice that the density of impurity charges is treated as continuous function in expressions (27)–(32). Meanwhile, we imply the number of donors N equal to 5–10. In other

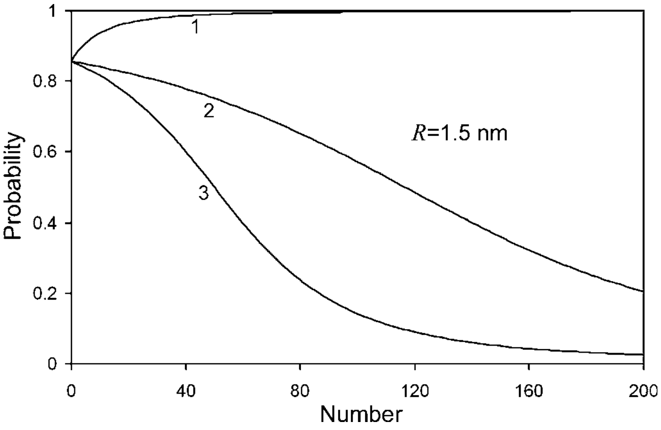

FIG. 8. The weight in the s-type envelope function for the homogeneous donor distribution in the nanocrystal for the (1) singlet, (2) doublet, and (3) triplet states versus the number of donors inside the nanocrystal.

case, if N is considerably greater, the perturbation originating from the central-cell interaction becomes not so small as well. As a result, the validity of the perturbative approach, based, in fact, on the two-level unperturbed system, is broken. We do not break the applicability of the perturbation theory but acquire some error of calculations when we use the model of continuous charge medium. Nevertheless, this error seems to be of the order of $1/N$, which does not exceed 10%–20% for the mentioned values N. We will restrict ourselves with that accuracy and apply the obtained expressions (27)–(32) for the description of the electron states in the nanocrystal containing several donors.

The behavior of the energy levels [Eq. (22)] depending on the dot radius R is presented in Fig. 7 for two different N. The singlet state has the lowest energy that is strongly split off from the two other levels. This provides a great value of the chemical shift similarly to the single-donor case. It is also seen that the level splitting and, consequently, the chemical shift increase almost proportionally to the number of donors in the dot.

At last, Fig. 8 shows the weights of the s-type envelope function of the singlet, doublet, and triplet states versus the number of donors N. Evidently, the s-type part of the wave function is dominant for all the states at small N. On the contrary, for large N, the s-part weights behave differently for the ground (singlet) and excited (doublet and triplet) states. In particular, the quota of the s-type envelope function in the singlet state gradually increases and approaches unity on increasing N. It means that in the case $N \gg 1$, the singlet state in the nanocrystal becomes similar to that in the bulk from the symmetry point of view. Meanwhile, the s-type part in the doublet and triplet states becomes more "light" as N increases. Moreover, their weights aspire to zero when $N \to \infty$. This circumstance drastically distinguishes the excited states in the dot and the bulk. Strictly speaking, we have no right, of course, to make any conclusions for $N \to \infty$ on the reason mentioned above. Therefore, we talk here not about the rigorous result but on the trend only.

VII. CONCLUSION

Summarizing our consideration, we would like to make some concluding remarks about the main features of the level splitting and chemical shift in silicon quantum dots with shallow donors. They can be formulated briefly as follows. (i) It has been revealed that the magnitude of the chemical shift in nanocrystals is much greater than that in bulk silicon. (ii) The splitting of the ground state and the chemical shift strongly depends on the nanocrystal size, which is a consequence of the quantum confinement effect in quantum dots. (iii) The donor position inside the nanocrystal crucially influences the degeneracy removal and chemical-shift value. In particular, if the donor takes up some off-center position, all energy levels turn out to be nondegenerate. However, this splitting becomes very small if the donor is placed at the dot boundary. At last, (iv) provided that the number of donors inside the dot becomes large, the ground electron state acquires the symmetry of the bulklike ground state. However, in contrast to bulk, the chemical shift remains great and increases as N increases.

ACKNOWLEDGMENTS

We thank the Russian Foundation for Basic Research and Ministry of Education and Science of the Russian Federation for the financial support of this work through Project No. 05-02-16762 and the program "Development of Scientific Potential of the High School" (Project No. 2.1.1.4022), respectively.

---

[1] F. Bassani, G. Iadonisi, and B. Preziosi, Rep. Prog. Phys. **37**, 1099 (1974).
[2] S. T. Pantelides, Rev. Mod. Phys. **50**, 797 (1978).
[3] M. Jaros, Adv. Phys. **29**, 409 (1980).
[4] M. Fujii, A. Mimura, S. Hayashi, and K. Yamamoto, Appl. Phys. Lett. **75**, 184 (1999).
[5] A. Mimura, M. Fujii, S. Hayashi, D. Kovalev, and F. Koch, Phys. Rev. B **62**, 12625 (2000).
[6] M. Fujii, Y. Yamaguchi, Y. Takase, K. Ninomiya, and S. Hayashi, Appl. Phys. Lett. **85**, 1158 (2004).
[7] D. I. Tetelbaum, S. A. Trushin, V. A. Burdov, A. I. Golovanov, D. G. Revin, and D. M. Gaponova, Nucl. Instrum. Methods Phys. Res. B **174**, 123 (2001).
[8] A. Kovalev, D. Wainstein, D. I. Tetelbaum, and A. N. Mikhailov, Surf. Interface Anal. **38**, 433 (2006).
[9] G. A. Kachurin, S. G. Cherkova, V. A. Volodin, V. G. Kesler, A. K. Gunakovsky, A. G. Cherkov, A. V. Bublikov, and D. I. Tetelbaum, Nucl. Instrum. Methods Phys. Res. B **222**, 497 (2004).
[10] T. Blomquist and G. Kirczenow, Phys. Rev. B **71**, 045301 (2005).
[11] G. Cantele, E. Degoli, E. Luppi, R. Magri, D. Ninno, G. Iadonisi, and S. Ossicini, Phys. Rev. B **72**, 113303 (2005).

[12] Y. Hada and M. Eto, Phys. Rev. B **68**, 155322 (2003).

[13] D. V. Melnikov and J. R. Chelikowsky, Phys. Rev. Lett. **92**, 046802 (2004).

[14] R. Tsu and D. Babic, Appl. Phys. Lett. **64**, 1806 (1994).

[15] M. Lannoo, C. Delerue, and G. Allan, Phys. Rev. Lett. **74**, 3415 (1995).

[16] R. Tsu, D. Babic, and L. Ioriatti, J. Appl. Phys. **82**, 1327 (1997).

[17] S. Ogut, R. Burdick, Y. Saad, and J. R. Chelikowsky, Phys. Rev. Lett. **90**, 127401 (2003).

[18] C. Delerue, M. Lannoo, and G. Allan, Phys. Rev. B **68**, 115411 (2003).

[19] X. Cartoixa and L.-W. Wang, Phys. Rev. Lett. **94**, 236804 (2005).

[20] F. Trani, D. Ninno, G. Cantele, G. Iadonisi, K. Hameeuw, E. Degoli, and S. Ossicini, Phys. Rev. B **73**, 245430 (2006).

[21] W. Kohn and J. M. Luttinger, Phys. Rev. **97**, 1721 (1955).

[22] W. Kohn and J. M. Luttinger, Phys. Rev. **98**, 915 (1955).

[23] A. Baldereshi, Phys. Rev. B **1**, 4673 (1970).

[24] S. T. Pantelides and C. T. Sah, Phys. Rev. B **10**, 621 (1974).

[25] Z. Zhou, M. L. Steigerwald, R. A. Friesner, L. Brus, and M. S. Hybertsen, Phys. Rev. B **71**, 245308 (2005).

[26] F. A. Reboredo, A. Franceschetti, and A. Zunger, Phys. Rev. B **61**, 13073 (2000).

[27] Y. M. Niquet, C. Delerue, G. Allan, and M. Lannoo, Phys. Rev. B **62**, 5109 (2000).

[28] S. Y. Ren, Phys. Rev. B **55**, 4665 (1997).

[29] B. Delley and E. F. Steigmeier, Phys. Rev. B **47**, 1397 (1993).

[30] V. A. Burdov, Zh. Eksp. Teor. Fiz. **121**, 480 (2002) [JETP **94**, 411 (2002)].

[31] A. S. Moskalenko, and I. N. Yassievich, Fiz. Tverd. Tela (S.-Peterburg) **46**, 1465 (2004) [Phys. Solid State **46**, 1508 (2004)].

[32] L.-W. Wang and A. Zunger, Phys. Rev. Lett. **73**, 1039 (1994).

[33] C. Delerue and M. Lannoo, *Nanostructures: Theory and Modelling* (Springer-Verlag, Berlin, 2004).

[34] A. A. Kopylov, Fiz. Tekh. Poluprovodn. (S.-Peterburg) **16**, 2141 (1982) **16**, 1380 (1982)].

[35] A. Blom, M. A. Odnoblyudov, I. N. Yassievich, and K.-A. Chao, Phys. Rev. B **68**, 165338 (2003).

[36] R. A. Faulkner, Phys. Rev. **184**, 713 (1969).